Engineering Science & Technology
http://ojs.wiserpub.com/index.php/EST/

UNIVERSAL WISER PUBLISHER

Research Article

Design and Analysis of the Low Bend Losses 2D Photonic Crystal Fiber-based Rhombic Ring Resonator for Magnetic Field Sensor

Aashis S Roy[1*], Ameena Parveen[2], Juhi Nishat Ansari[3]

[1]Department of Chemistry, S. S.Tegnoor Degree College, Gubbi Colony-585104, India
[2]Department of Physics, Government Degree College, Yadgir 585201, India
[3]Department of Electronics & Communication, KCT Engineering College, Kalaburagi, India
Email: aashisroy@gmail.com

Received: 12 June 2023; **Revised:** 24 July 2023; **Accepted:** 9 August 2023

Abstract: We designed and analyzed a magnetic field sensor with low bend losses 2D photonic crystal fiber based on a rhombic ring resonator. The proposed design consists of silicon rods with a diameter of 200 nm in the X and Z directions, which are 61 × 61 silicon rods. The Refractive Index (RI) of silicon is n = 3.48 at λ = 1.55 mm and the number of air holes along the direction is 33 × 33. It was found that the photonic crystal fibers used the photonic band gap phenomenon to guide light but rather an area of the fiber core with a lower refractive index of 0.9 nm. It is important to note that there are low bend losses in 2D photonic crystal fibers, enabling response to small changes in the magnetic fluid viscosity, refractive index, and other physical parameters. The flow of electromagnetic energy, indicated by the Poynting vector (s), indicates that the magnitude of the power carrier per unit area in the direction of S is approximately 1.23 W/m^2.

***Keywords*:** photonic crystal fiber, rhombic ring resonator, magnetic field sensor, poynting vector, refractive index

1. Introduction

Photonic Crystal Fibers (PCFs) have been an important research field for two decades because of their low-loss dielectric medium, low-index core, light weight, compactness, and fast rate of data transmission with low energy consumption. PCFs are periodic nanostructured low- and high-refractive-index materials used in a wide range of sensing applications such as temperature, pressure, magnetic field, electric field, refractive index, and chemical and biochemical sensors [1], [2]. Among all the PCFs-based optical sensors, infiltrated magnetic sensors have attracted research into the creation of a highly sensitive magnetic field sensor with low noise and electromagnetic interference [3]. Photonic crystal fiber-based magnetic field sensors are promising alternatives to conventional sensors because of their small size, low electromagnetic interference, remote monitoring and enhancement through optical network modalities, high consistency, and sensitivity [4]. While other systems rely on changes in the state of light polarization, the first fiber-optic magnetic field sensors developed in the last two decades used magnetostrictive materials along with a Mach-Zehnder interferometer [5], [6].

Magnetic Fluid (MF) is a liquid that is typically made up of single-domain magnetic particles encapsulated with a Multifunctional Surfactant (MFS) to make a suspended optical fluid, resulting in alterations of physiochemical

DOI: https://doi.org/10.37256/est.5120243210

properties, including refractive index, magnetic susceptibility, polydispersity, and bipolar interaction. Many fiber-optic magnetic field sensors have been proposed based on different sensing technologies such as multimode interference, Fabry-Perot interference, grating optics, Sagnac interference, and surface plasma resonance [7]. These sensors function by introducing MF into the inner holes of the microstructured fiber or coating the surface of the specialty fiber with MF. By observing the wavelength shift of the peak/valley in the output spectrum, the strength of the magnetic field is typically determined. Although these sensors have demonstrated excellent sensing capabilities, their output spectral visibility is typically low, and the Full Width at Half Maximum (FWHM) of the valley/peak is typically wide, which leads to a low measurement resolution of the magnetic field and limited measurement accuracy [8], [9]. MFSs are used to detect MF, which is a blend of iron with oil, water, or any liquid. Magnetic field detection is a significant issue in many applications, such as defense, navigation, and industry. The sensors used for screening can be vulnerable to Electromagnetic Interference (EMI), but because of the benefits over conventional sensors, photonic crystal-based sensors could be a phenomenal option. Moreover, magnetic fluids are useful materials with extraordinary properties including birefringence, refractive index, and field-dependent transmission [10]-[12]. The magnetic field sensitive experimental results demonstrate that the proposed sensor based on a wedge-shaped fiber tip has great potential for realizing lab-on-fiber devices and applications because the magnetic field intensity and direction sensitivities of the magnetic field sensors based on Multimode Fiber (MMF) and Few-Mode Fiber (FMF) are 2,317 pm/mT, 497 pm/° and 6,776 pm/mT, 2,313 pm/°, respectively studied by Wang et al. [13]. It is also evident that MF to the external magnetic field can be used to sense magnetic field intensity and direction via monitoring the dip wavelength of Surface Plasmon Resonance (SPR). The obtained Refractive Index (RI) sensitivities are 2,105 nm/RIU (RI range: 1.332-1.365) and 6,692 nm/RIU (RI range: 1.372-1.411), magnetic field intensity sensitivities are 11.67 nm/mT (0°), and -0.47 nm/mT (90°). Besides, the proposed sensing probe is ultracompact and the footprint is extremely small (the length of the sensing part is only 615 μm), which is very helpful for magnetic field detection in narrow space and gradient fields as mentioned by Hao et al. [14].

In this study, we designed and analyzed a low-bend-loss 2D photonic crystal fiber-based rhombic ring resonator for magnetic field sensors. This design will be useful in fiber optic innovation, which is essential for media transmission applications.

2. Theoretical model of PCFs

The basic structure of a magnetic fluid sensor consists of a rhombic ring resonator lattice of air holes radius is r = 0.37 mm and the rhombic ring size is around 17 × 17 mm, where lattice constant ‘a’ is taken as 355 nm which is the distance between centers of two adjacent air holes. The silicon refractive index is n = 3.48 at λ = 1.55 mm and the number of air holes in the X and Z directions are 61 × 61 silicon rods as shown in Figure 1. The lattice constant and radius of the circular hole have been chosen to maximize the photonic band gap around the reference wavelength of 1,340 nm. In this lattice, a rhombic ring resonator is created coupled with an inline quasi-waveguide that produces a narrow peak in the transmission spectrum that is used to detect the magnetic flux. The incident source is a Gauss impulse light source located at the input of the waveguide and the detector is placed at the end of the waveguide [15], [16].

The photonic crystal fiber-based rhombic ring resonator sensor is a novel and promising technology that has shown great potential in the field of magnetic field sensing. By utilizing the unique properties of photonic crystal fibers and the resonant characteristics of rhombic ring structures, this sensor offers several advantages over traditional magnetic field sensors. Firstly, the photonic crystal-based sensor provides better sensitivity and selectivity compared to conventional optical fiber methods [17]. This is due to the index of refractive variation with respect to a change in the sensing element, which is enhanced by using the ring resonator photonic crystal structure. Secondly, the combination of photonic crystal fiber with surface plasmon resonance in this sensor design offers a flexible structure that is highly resistant to electromagnetic interference. This feature ensures accurate and reliable measurements even in challenging environments. Lastly, the integration and mechanical stability of this sensor make it a viable option for various application scenarios [18]. One of the most important factors is considering when dealing with the viscosity of the filling substance. Viscosity and capillary forces have a significant impact on the infiltration time. For instance, the viscous properties of Liquid Chromatography (LC) and polymers are completely different and highly dependent on temperature

and curing. Sometimes, the capillary forces are strong enough to fill the Photonic Crystal Fiber (PCF) microcapillaries, but other times, applying pressure with vacuum chambers is required [19]. Finally, although there are techniques that greatly assist, there is no need for any type of material-specific gas infiltration process. The following subsections provide information on the available infiltration methods for all three cases [20].

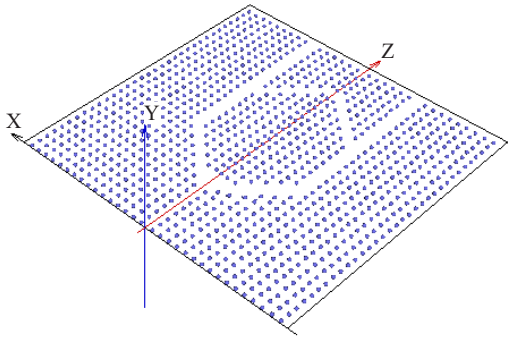

Figure 1. Schematic diagram of PhC-based sensor

3. Sensing principle

The principle is based on the Faraday Effect by assessing the Faraday rotation angle (θ_F), and the detection of the magnetic field is performed as indicated in Equation 1.

$$\theta_F = VH_{ext}L \tag{1}$$

Where L is the length of the propagated light wave, V is the Verdet constant, and H_{ext} is the magnetic field(external), which is the outcome of the imaginary elements ($\pm j_g$). For a gyro tropic medium magnetized along the x-direction, the permittivity of the sensor (ϵ) is given by Equation 2.

$$\epsilon = \begin{bmatrix} \epsilon_{xx} & j_g & 0 \\ -j_g & \epsilon_{yy} & 0 \\ 0 & 0 & \epsilon_{zz} \end{bmatrix} \tag{2}$$

Where the magneto-optic permittivity parameters $\epsilon_{xx} = \epsilon_{yy} = \epsilon_{zz}$ are real. In a first approximation, the gyrotropy parameter (g), is directly proportional to H_{ext}, according to Equation 3,

$$g = \epsilon_0 \chi H_{ext} \tag{3}$$

where χ is the magneto-optic susceptibility in H_{ext}, and ϵ_0 is the permittivity in a vacuum. The intensity of the transmitted light wave changed when H_{ext} was applied to a photonic fiber source. The variation in the intensity corresponds to the relationship between H_{ext} and θ_F. Therefore, H_{ext} can be calculated by noting the decrease in light wave intensity [21]-[24].

4. Results and discussion

Figure 2 shows the refractive index of the infiltrated magnetic fluid as a function of the electric field applied. It is

observed that the photonic crystal fibers use the photonic bandgap phenomenon, which does not guide light but rather an area of the fiber core with a lower refractive index of 0.9 nm. Therefore, the guided system operated over a longer wavelength range. It is possible that the refractive index of the core was lower than that of the cladding structure. If the core is hollow, the refractive index is equal to that of air. Such types of hollow-core photonic bandgap fibers may be employed for directing light in spectral ranges where the absorption in silicon is relatively significant because most of the light then travels in air rather than in silicon [25], [26].

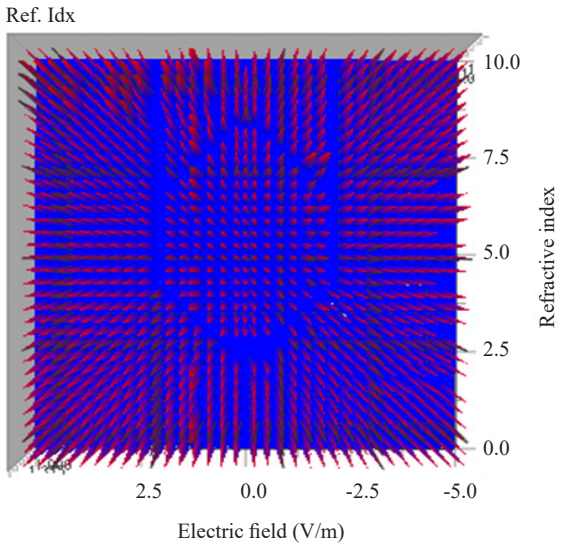

Figure 2. Variation of the refractive index without infiltrated magnetic fluid in the PhC fibers

The magnetic field response without infiltrated magnetic fluid in the photonic crystal fibers is shown in Figure 3. An electromagnetic wave can propagate in a PCF without significantly broadening or changing its beam profile, and without the aid of a bandgap or other manufactured flaws such as waveguides, as shown in Figure 3(a). This process is known as the self-guiding of light. This phenomenon takes place as a result of the planar photonic crystal's intricate spatial dispersion characteristics, which cause anomalous light refraction in a rhombic ring resonator. Figure 3(b) shows the real-imaginary parts of the electric field in the x- and z-components along the resultant direction, and the numerical and simulated results show excellent agreement with the solenoidal vector field, that is, the field line extends to infinity or warp around the closed curve path [27], [28]. It observed that the electric field desiccates when the magnetic field is applied from 9.8 V/m to 4.46 V/m due to the increase in the dielectric polarization. Here, the electric field is stronger than the magnetic field may be due to the electromagnetic waves incident on an atom it will often see the poles of the electrons, whereas the magnetic can only interact with the magnetic dipoles of the atoms, etc. which are much weaker in nature. The magnetic field shows that the magnetic influences the electric binary signals without changing any band gap or amplitude of the signal which helps the transmission of signal with lower bandwidth that helps in the sensing application as shown in Figure 3(c). In the absence of infiltrated magnetic fluid into the PhC fibers, there is no change in the energy of the output signal, as shown in Figure 3(d). It is observed that the energy associated with the magnetic field is equal to the energy of the electric field of the electromagnetic waves that it may be the polarized charges particles oscillates in the same plane wave.

The magnetic field response with the infiltrated magnetic fluids filled in the photonic crystal fibers as shown in Figure 4. An electromagnetic wave can propagate in a PCF with significant enhancement or by changing its beam profile, and by lowering the bandgap or other manufactured flaws such as waveguides with self-guiding of light, as shown in Figure 4(a). This phenomenon occurs as a result of the planar photonic crystal's intricate spatial dispersion characteristics of the magnetic fluid, which causes anomalous light refraction into two paths from a rhombic ring resonator. Figure 4(b) shows the real-imaginary parts of the electric field in the x- and z-components along the resultant

direction, and the numerical and simulated results show excellent agreement with the solenoidal vector field into the higher amplitude in the binary signal [29]-[31]. The magnetic field shows that the magnetic influences the electric binary signals by changing any band gap or amplitude of the signal which helps the transmission of signal with lower bandwidth that helps in the sensing application as shown in Figure 4(c). It is noted that in the absence of magnetic fluid infiltration into the PhC fibers, there was a change in energy in the output signal, as shown in Figure 4(d). The energy associated with electromagnetic waves with an electric field is higher than the external magnetic field and may be oscillating in different planes because the electric component of the Lorentz force will be vastly bigger than the magnetic part.

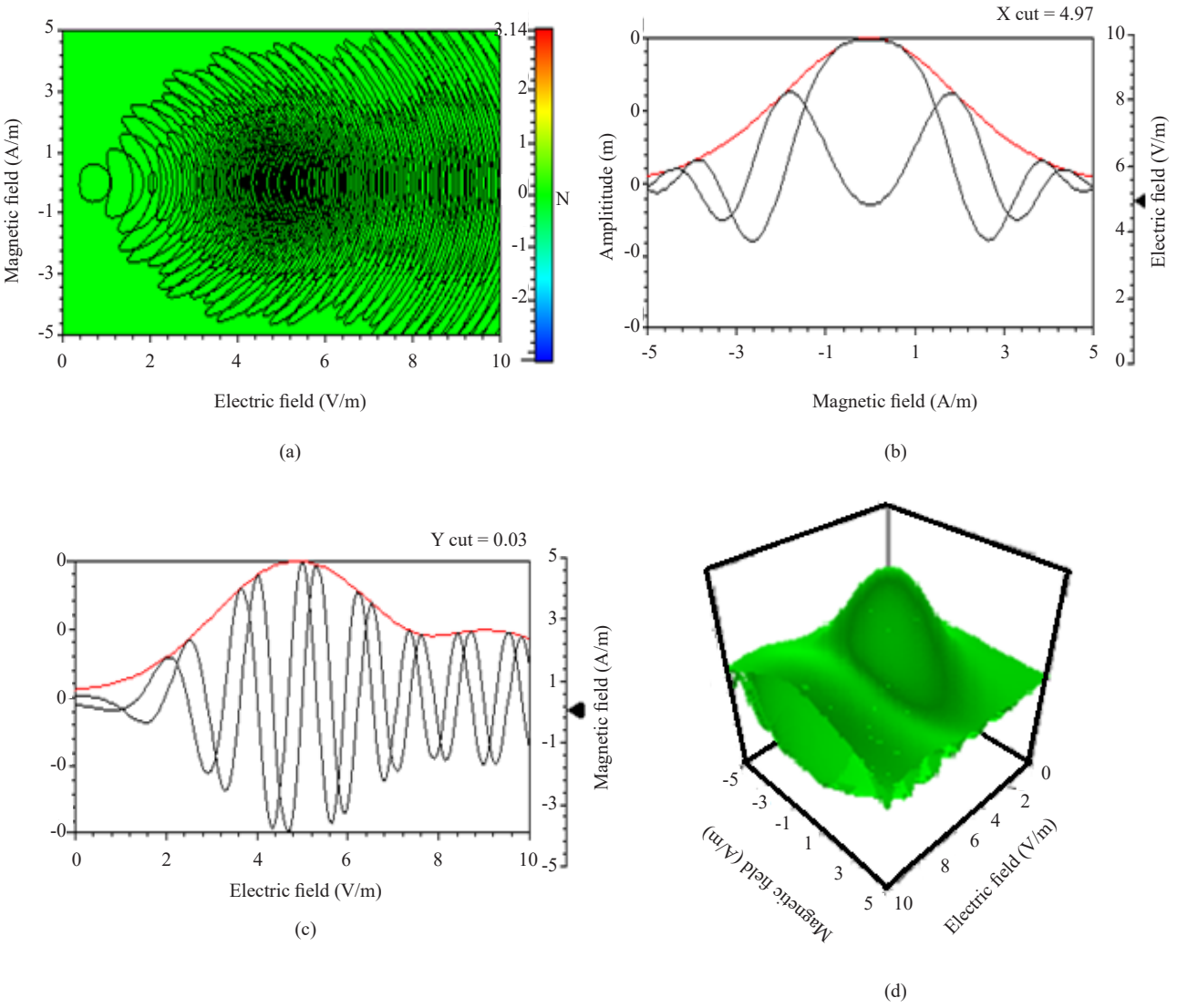

Figure 3. The magnetic field response of (a) variation of binary signals in designed PCFs, (b) real-imaginary electric field, (c) real-imaginary resultant magnetic field, and (d) change in amplitude without infiltrated magnetic fluid in PCFs

The resonant power dissipated as a function of time for the infiltrated magnetic fluid in the PhCs as shown in Figure 5. It is important to note that there is low bend loss in 2D photonic crystal fibers around ±0.01 eV that can respond to small changes in the magnetic fluid viscosity, and the refractive index may be due to the negligible dielectric polarization in the materials. Therefore, it is also evident that the applied periodic force does not alter the amplitude, and the peak in the gain at all times at a certain applied frequency range remains the same [32].

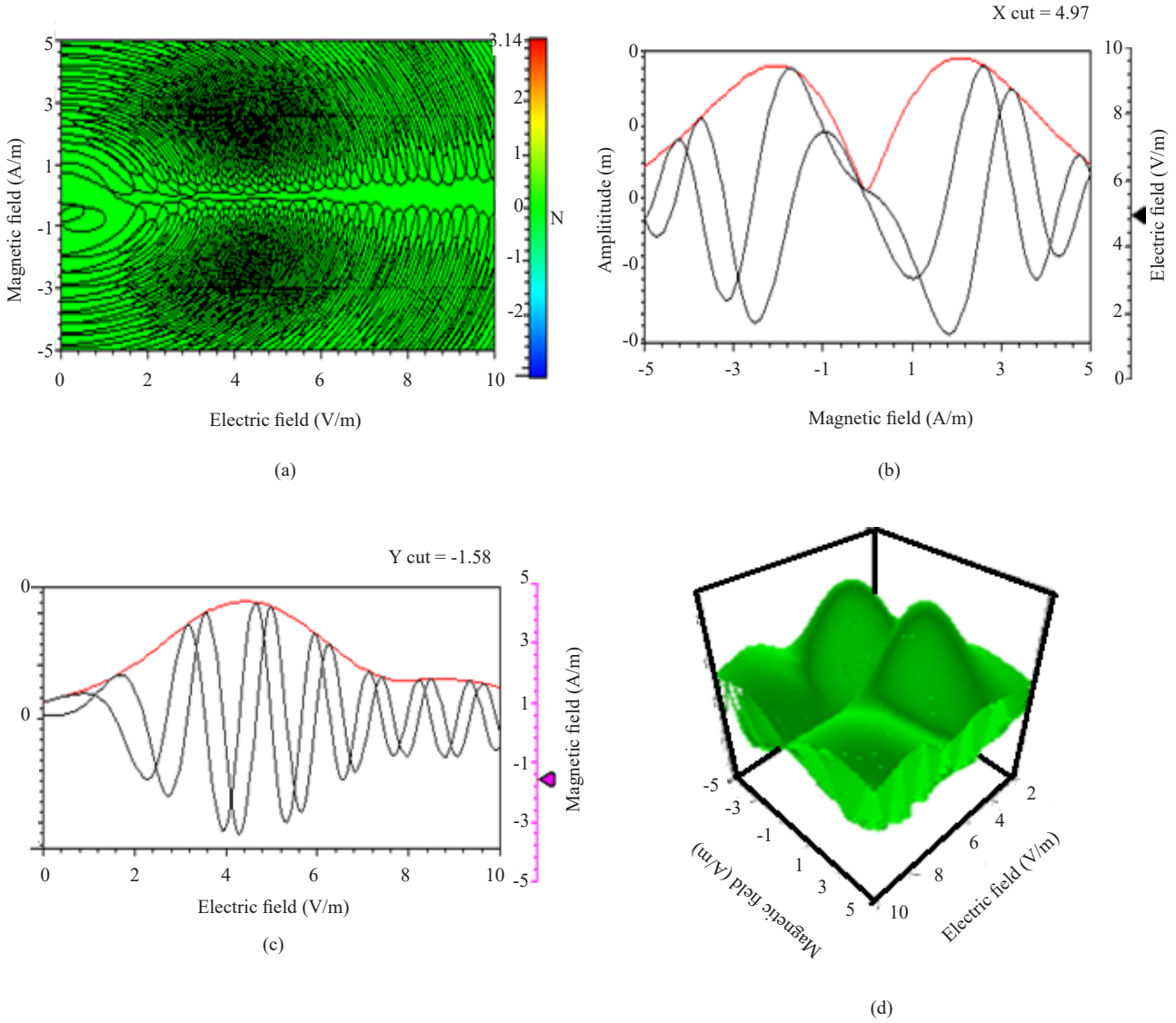

Figure 4. The magnetic field response of (a) variation of binary signals in designed PCFs, (b) real-imaginary electric field, (c) real-imaginary magnetic field, and (d) change in amplitude with infiltrated magnetic fluid in PCFs

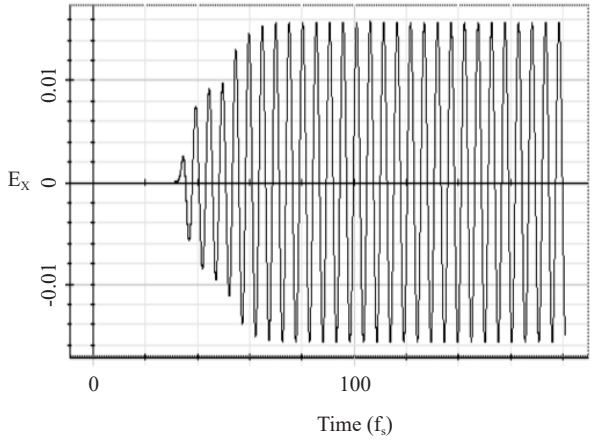

Figure 5. The power dissipated as a function of time

Figure 6 illustrates the variation in the refractive index with the resonant wavelength. The resonant wavelength increased with an increase in the refractive index from 1.468 nm to 1.484 nm. This may be due to the pleasance of the magnetic fluid, which suppresses the electric field and reduces noise. The Fast Fourier Transform was used to estimate the normalized transmission spectra at the output port "B" of the proposed double BPF (FFT). The Finite-Difference Time-Domain (FDTD) approach was used to calculate the electric (E) and magnetic (H) field components in two dimensions. It was demonstrated that as the RI increases, the resonant peak of the rhombic ring resonator gradually moves toward a higher wavelength [33].

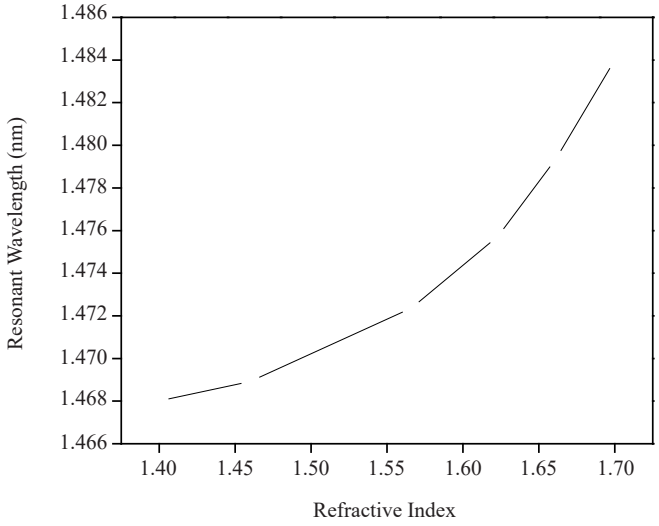

Figure 6. Variation of refractive index with resonant wavelength

Figure 7 shows the variation in the quality factor and magnetic field sensitivity with resonant wavelength. The quality factor decreases with an increase in the resonance frequency, which may be due to the relative evanescent field at the rhombic ring resonator. We notice that the optical field is stronger in the innermost holes of the center resonant ring. Owing to the significant amount of light-matter interactions present inside them, the rhombic resonant ring is extremely sensitive to changes in the refractive index. It was observed that at a wavelength of 1,618 nm, the sensitivity was 104 nm/Oe and the quality factor was 8,756. It is also important to note that the magnetic field sensitivity increases because of the dominance of electromagnetic resonance in the rhombic ring resonator [34]. The modeling represents a fiber with r_0 = 0.4 m and Pitch = 1.0 m. Anomalous dispersion properties ($\beta_2 < 0$) exist for a wide range of wavelengths. This interval is increased for r_2 = 0.79 m from 0.38 to 1.24 m, but not for r_2 = 0.2 m. For wavelengths over 0.77 m, we have a dispersion-flattened photonic crystal fiber. The point source was positioned at the terminus of the photonic crystal fiber. The crystal structure was superimposed on the map field because the produced light beam was concentrated in the direction of the fold.

The azimuthal mode-pointing vector (S) against the magnetic field profiles at 940 nm is shown in Figure 8. The azimuthal Poynting vector was found to be continuous, whereas the Poynting vector of the radially polarized mode was discontinuous at both the inner and outer core boundaries (TM boundary conditions). The phase indices nr = 2.58 and na = 3.75, result in a cylindrical birefringence of 0.010, which is slightly lower than the step-index model's prediction. The HE21 hybrid mode in typical step-index fibers is related to the third mode, which has a phase index of 1.132 [35]. The flow of electromagnetic energy, indicated by the Poynting vector (s), indicates that the magnitude of the power carrier per unit area in the direction of S is approximately 1.23 W/m^2. Although the Poynting vector distributions of the radially polarized mode and phase index are very similar to those of the HE21 mode, the vector field distributions are noticeably different.

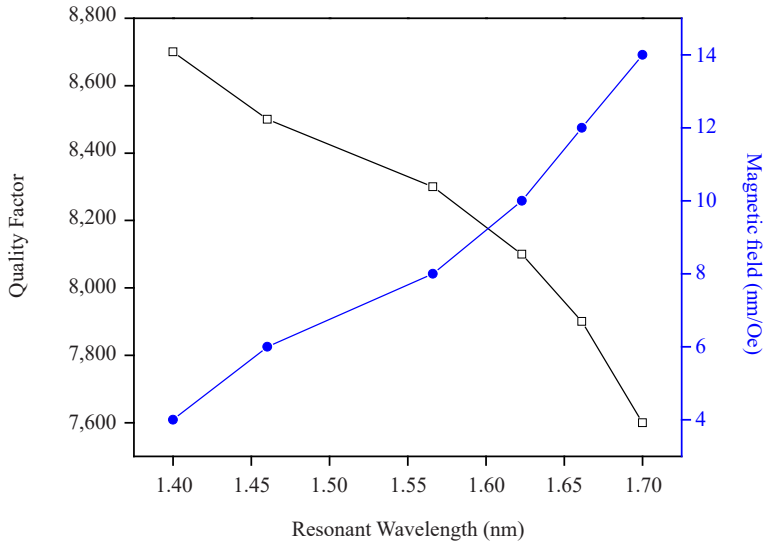

Figure 7. Variation of Q-factor and magnetic field sensitivity with resonant wavelength

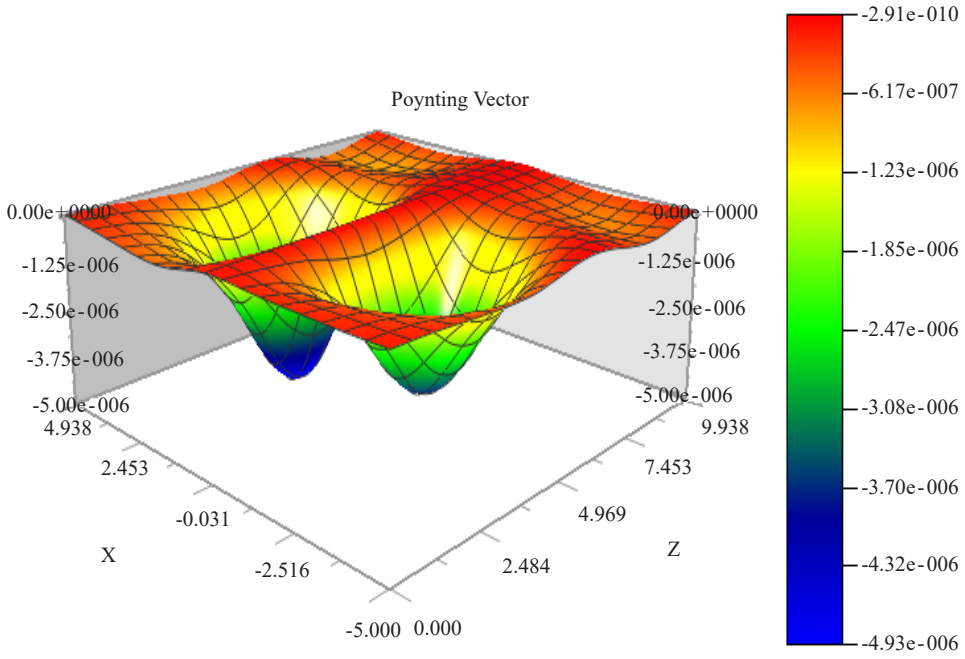

Figure 8. Variation of the azimuthal mode pointing vector

5. Conclusion

The proposed design consists of silicon rods with a diameter of 200 nm in the X and Z directions are 61 × 61 silicon rods, the rhombic ring size is around 17 × 17 mm and the RI of silicon is n = 3.48 at λ = 1.55. It was confirmed that the photonic crystal fibers used the photonic band gap phenomenon to guide light but rather an area of the fiber core with a lower refractive index of 0.9 nm. The magnetic field response with infiltrated magnetic fluid can propagate in a PCF with significantly enhanced or changing beam profile, and lowering the bandgap confirm that the electric field desiccates with the magnetic field from 9.8 V/m to 4.46 V/m due to the increases in dielectric polarization. However, the

electric and magnetic field energy associated with the electromagnetic wave is the same. The rhombic resonant ring is very sensitive to refractive index changes owing to the large degree of light-matter interactions inside it. Magnetic field sensors confirmed a low-bend-loss 2D photonic crystal fiber is about ±0.01 eV based on a rhombic ring resonator. The quality factor indicates that the external field in PCFs does not have much effect even after a longer period was 8,756. The flow of electromagnetic energy indicated by the Poynting vector (s) indicates that the magnitude of the power carrier per unit area in the direction of S is about 1.23 W/m^2.

Project funding

No funds available for this study from any agencies.

Data availability

Data underlying the results presented in this paper are not publicly available at the time of publication, which may be obtained from the authors upon reasonable request.

Conflict of interest

The authors declare no conflicts of interest.

Reference

[1] R. Gao, Y. Jiang, and S. Abdelaziz, "All-fiber magnetic field sensors based on magnetic fluid-filled photonic crystal fibers," *Optics Letters*, vol. 38, no. 9, pp. 1539-1541, 2013.
[2] J. Wang, L. Pei, J. S. Wang, Z. L. Ruan, J. J. Zheng, J. Li, and T. G. Ning, "Magnetic field and temperature dual-parameter sensor based on magnetic fluid materials filled photonic crystal fiber," *Optics Express*, vol. 28, no. 2, pp. 1456-1471, 2020.
[3] X. Z. Ding, H-Z. Yang, X-G. Qiao, P. Zhang, O. Tian, Q. Z. Rong, N. A. M. Nazal, K-S Lim, and H. Ahmad, "Mach-Zehnder interferometric magnetic field sensor based on a photonic crystal fiber and magnetic fluid," *Applied Optics*, vol. 57, no. 9, pp. 2050-2056, 2018.
[4] J. Zheng, X. Y. Dong, P. Zu, L. Y. Shao, C. C. Chan, Y. Cui, and P. P. Shum, "Magnetic field sensor using tilted fiber grating interacting with magnetic fluid," *Optics Express*, vol. 21, no. 15, pp. 17863-17868, 2013.
[5] Y. Zhao, D. Wu, R.-Q. Lv, and Y. Ying, "Tunable characteristics and mechanism analysis of the magnetic fluid refractive index with applied magnetic field," *IEEE Transactions on Magnetics*, vol. 50, no. 8, pp. 1-5, 2014.
[6] B. T. Tung, D. V. Dao, T. Ikeda, Y. Kanamori, K. Hane, and S. Sugiyama, "Investigation of strain sensing effect in modified single-defect photonic crystal nanocavity," *Optics Express*, vol. 19, no. 9, pp. 8821-8829, 2011.
[7] T. T. Mai, F. L. Hsiao, C. Lee, W. Xiang, C. C. Chen, and W. K. Choi, "Optimization and comparison of photonic crystal resonators for silicon micro-cantilever sensor," *Sensors and Actuators*, vol. 165, no. 1, pp. 16-25, 2011.
[8] R.-Q. Lv, Y. Zhao, D. Wang, and Q. Wang, "Magnetic fluid-filled optical fiber Fabry-Pérot sensor for magnetic field measurement," *IEEE Photonics Technology Letters*, vol. 26, no. 3, pp. 217-219, 2014.
[9] A. M. Upadhyaya, P. Sharan, and M. C. Srivastava, "Micro-opto-electro-mechanical system based microcantilever sensor for biosensing applications," *Journal of the Optical Society of America B*, vol. 39, no. 7, pp. 1736-1742, 2022.
[10] H. V. Thakur, S. M. Nalawade, S. Gupta, R. Kitture, and S. N. Kale, "Photonic crystal fiber injected with Fe_3O_4 nanofluid for magnetic field detection," *Applied Physics Letter*, vol. 99, no. 6, pp. 161101, 2011.
[11] X. Li and H. Ding, "All-fiber magnetic-field sensor based on microfiber knot resonator and magnetic fluid," *Optics Letter*, vol. 37, no. 24, pp. 5187-5189, 2012.
[12] T. Tanabe, K. Nishiguchi, E. Kuramochi, and M. Notomi, "Low power and fast electro-optic silicon modulator with lateral p-i-n embedded photonic crystal nanocavity," *Optics Express*, vol. 17, no. 25, pp. 22505-22513, 2009.

[13] J. Wang, S. L. Pu, Z. J. Hao, C. C. Zhang, W. N. Liu, and Y. Y. Fan, "Comparative study of lab-on-fiber vector magnetic field sensor based on multimode and few-mode fiber," *Measurement*, vol. 207, pp. 112441, 2023.
[14] Z. J. Hao, Y. X. Li, S. L. Pu, J. Wang, F. Chen, and M. Lahoubi, "Ultrahigh-performance vector magnetic field sensor with wedge-shaped fiber tip based on surface plasmon resonance and magnetic fluid," *Nanophotonics*, vol. 11, no. 15, pp. 3519-3528, 2022.
[15] C. C. Zhang, S. L. Pu, Z. J. Hao, B. Y. Wang, M. Yuan, and Y. X. Zhang, "Magnetic field sensing based on whispering gallery mode with nanostructured magnetic fluid-infiltrated photonic crystal fiber," *Nanomaterials*, vol. 12, no. 5, pp. 862-872, 2022.
[16] H. T. Wang, S. L. Pu, N. Wang, S. H. Dong, and J. Huang, "Magnetic field sensing based on singlemode-multimode-singlemode fiber structures using magnetic fluids as cladding," *Optics Letter*, vol. 38, no. 19, pp. 3765-3768, 2013.
[17] S. H. Dong, S. L. Pu, and H. T. Wang, "Magnetic field sensing based on magnetic-fluid-clad fiber-optic structure with taper-like and lateral-offset fusion splicing," *Optics Express*, vol. 22, no. 16, pp. 19108-19116, 2014.
[18] T. Hu, Y. Zhao, X. Li, J. Chen, and Z. Lv, "Novel optical fiber current sensor based on magnetic fluid," *Chinese Optics Letter*, vol. 8, no. 4, pp. 392-394, 2010.
[19] J. Dai, M. Yang, X. Li, H. Liu, and X. Tong, "Magnetic field sensor based on magnetic fluid clad etched fiber Bragg grating," *Optical Fiber Technology*, vol. 17, no. 3, pp. 210-213, 2011.
[20] Y. Yu, X. Li, X. Hong, Y. Deng, K. Song, Y. Geng, H. Wei, and W. Tong, "Some features of the photonic crystal fiber temperature sensor with liquid ethanol filling," *Optics Express*, vol. 18, no. 15, pp. 15383-15388, 2010.
[21] F. Abdelmalek, "Design of A novel left-handed photonic crystal sensor operating in aqueous environment," *IEEE Photonics Technology*, vol. 23, no. 3, pp. 188-190, 2011.
[22] C. Lee, A. Sueh, P. Yee, J. L. Perera, C. Chen, and N. Balasubramanian, "Design of nanobiophotonics resonators for biomolecules detection," In 2008 3rd IEEE International Conference on Nano/Micro Engineered and Molecular Systems, Sanya, 2008, pp. 274-279.
[23] H. Alipour-Banaei and F. Mehdizadeh, "A proposal for anti-UVB filter based on one dimensional photonic crystal structure," *Journal of Nanomaterials & Biostructures*, vol. 7, no. 1, pp. 361-371, 2012.
[24] X. Zhang, Q. Liao, T. Yu, N. Liu, and Y. Huang, "Novel ultracompact wavelength division demultiplexer based on photonic band gap," *Optics Communication*, vol. 285, no. 3, pp. 274-276, 2012.
[25] S. Ahmed, S. Y. Shi, D. W. Prather, and R. A. Soref, "Electro optical switching using coupled PC waveguides," *Optics Express*, vol. 10, no. 20, pp. 1048-1059, 2002.
[26] L. A. DeLouise, P. M. Kou, and B. L. Miller, "Cross-correlation of optical microcavity biosensor response with immobilized enzyme activity Insights into biosensor sensitivity," *Analytical Chemistry*, vol. 77, no. 10, pp. 3222-3230, 2005.
[27] P. Andalib and N. Granpayeh, "All optical ultracompact photonic crystal and gate based on nonlinear ring resonator," *Journal of the Optical Society of America B*, vol. 26, no. 1, pp. 10-16, 2009.
[28] M. F. O. Hameed, M. Abdelrazzak, and S. S. A. Obayya, "Novel design of ultra-compact triangular lattice silica photonic crystal polarization converter," *IEEE Journal Light Wave Technology*, vol. 31, no. 1, pp. 81-86, 2013.
[29] F. Hsiao and C. Lee, "Computational study of photonic crystals nano-ring resonator for biochemical sensing," *IEEE Sensors*, vol. 10, no. 7, pp. 1185-1191, 2010.
[30] S. Olyaee, S. Najafgholinezhad, and H. Alipour Banaei, "Four-channel label-free photonic crystal biosensor using nano cavity resonators," *Photonic Sensors*, vol. 3, pp. 231-236, 2013.
[31] S. Pal, E. Guillermain, R. Sriram, B. L. Miller, and P. M. Fauchet, "Silicon photonic crystal nano cavity coupled waveguides for error-corrected optical biosensing," *Biosensors and Bioelectronics*, vol. 26, no. 10, pp. 4024-4031, 2011.
[32] D. Dorfner, T. Zabel, T. Hurlimann, N. Hauke, L. Frandsen, U. Rant, G. Abstreiter, and J. Finley, "Photonic crystal nanostructures for optical biosensing applications," *Biosensors and Bioelectronics*, vol. 24, no. 12, pp. 3688-3692, 2009.
[33] M. B. Hossain, I. M. Mehedi, M. Moznuzzaman, L. F. Abdulrazak, and M. A. Hossain, "High performance refractive index SPR sensor modeling employing graphene tri sheets," *Results in Physics*, vol. 15, pp. 102719, 2019.
[34] S. Mehta, S. Vankalkunti, P. K. Kachhap, P. R. Gautam, and M. Singh, "Sensitivity improvement of photonic crystal refractive index sensor using porous silicon nano rods," *Materials Science in Semiconductor Processing*, vol. 165, pp. 107687, 2023.
[35] Y. H. Zhang, Z. Z. Liang, D. J. Meng, Z. Qin, Y. D. Fan, X. Y. Shi, D. R. Smith, and E. Z. Hou, "All-dielectric

refractive index sensor based on Fano resonance with high sensitivity in the mid-infrared region," *Results in Physics*, vol. 24, pp. 104129, 2021.